Synthesis and cyclic voltammetry of $CrFe_2O_4/(MWCNTs)_x$ nanohybrids

Mubasher, M. Mumtaz, Mehwish Hassan, Najeeb Ur Rehman Lashari, Zubair Ahmad, M. Tahir Khan & M. Ali

Journal of Materials Science: Materials in Electronics

ISSN 0957-4522

J Mater Sci: Mater Electron
DOI 10.1007/s10854-020-03950-2

Springer

Journal of Materials Science: Materials in Electronics
https://doi.org/10.1007/s10854-020-03950-2

Synthesis and cyclic voltammetry of $CrFe_2O_4$/$(MWCNTs)_x$ nanohybrids

Mubasher[1] · M. Mumtaz[1] · Mehwish Hassan[2] · Najeeb Ur Rehman Lashari[3] · Zubair Ahmad[4] · M. Tahir Khan[5] · M. Ali[1]

Received: 22 April 2020 / Accepted: 6 July 2020

Abstract
The chemical co-precipitation route was opted for the synthesis of chromium ferrite ($CrFe_2O_4$) nanoparticles and the pristine multi-walled carbon nanotubes (MWCNTs) were used for the preparation of desired $CrFe_2O_4$/$(MWCNTs)_x$; $x = 0$, 5, 10, 15, and 20 wt% nanohybrids using the ultra-sonication method. Toluene was used for the first time as dispersive medium for the preparation of these nanohybrids. The crystalline structure, morphology, vibrational modes, and electrochemical performance of these nanohybrids were characterized by using X-ray diffraction (XRD), Raman spectroscopy, scanning electron microscope (SEM), energy dispersive X-ray spectroscopy, Fourier transform infrared spectroscopy, electrochemical impedance spectroscopy (EIS), and cyclic voltammetry. The structural properties of pristine MWCNTs, $CrFe_2O_4$ nanoparticles, and $CrFe_2O_4$/$(MWCNTs)_x$ nanohybrids are evaluated by XRD and Raman spectroscopy. The SEM images presented the attachment of $CrFe_2O_4$ nanoparticles on the surface of MWCNTs. The specific capacitance was decreased with increasing number of cycles, while it was observed to be increased with increasing MWCNTs content. From EIS, the decrease in charge transfer resistance was observed with the increased loadings of MWCNTs, which showed the enhanced electrochemical behavior of these nanohybrids. Therefore, the significant improvement in electrochemical properties showed that these nanohybrids can be promising candidates for energy storage devices like lithium-ion (Li-ion) batteries.

1 Introduction

In recent times, researchers are focusing on the production of high-energy storage devices that got maximum power deliverance and bearability. The subsequent generations need maximum energy, high power, smart range, and ecologically friendly storage devices for various applications [1–4]. Li-ion batteries presently signify its importance in portable electronics market as rechargeable batteries or large-scale electrical grids that require high power densities and higher energy [5–7]. The electrochemical performance of a material can be constrained with electrolyte, current collector, electrode material, and the separator [8]. Transition metal oxides (TMOs) bear high theoretical capacity in contrast to conventional graphite, resulting in great interest as storage devices [9, 10]. The iron-based materials have been widely used in various applications like catalyst medical, magnetic resonance imaging, and energy storage devices [11–17]. The diverse morphology of ferrites-based materials revealed high electrochemical properties [18]. Ferrite nanoparticles can be produced in sponge-like shapes by numerous routes like co-precipitation, sonochemical, hydrothermal, sol-gel, solvothermal method, and nanocasting [19–21]. Poor cyclic performance is the main challenge in using iron-based materials, which is the point of interest to be investigated. The pseudo behavior of charge storage for hydroxides, selenides, metal oxides, sulfides, and conductive polymers takes place due to fast reversible surface faradic reactions at electrolyte interface [22–25]. Diverse studies have been made to investigate the formation of composites along with conductive materials like MWCNTs, single-walled carbon nanotubes (SWCNTs), carbon nanoplatelets, reduced

✉ M. Mumtaz
mmumtaz75@yahoo.com

[1] Materials Research Laboratory, Department of Physics, Faculty of Basic and Applied Sciences (FBAS), International Islamic University (IIU), H-10, Islamabad 44000, Pakistan

[2] Department of Sciences and Humanities, FAST, NUCES, Islamabad, Pakistan

[3] School of Material Science and Engineering, Xian Polytechnic University, Xian 710048, Shaanxi, China

[4] Ibn-e-Sina Institute of Technology, H-11/4, Islamabad, Pakistan

[5] Department of Physics, Faculty of Engineering and Applied Sciences, Riphah International University, I-14, Islamabad 44000, Pakistan

Published online: 13 July 2020

graphene, graphene oxide, and carbon nanofibers [26–33]. The Cr-based ferrite nanoparticles exhibit high theoretical capacity, eco-friendly, high abundance, large volume variation, and poor electronic conductivity [34–36]. The electrochemical performance of bare α-Fe_2O_3 nanoparticles was significantly improved with the addition of MWCNTs. The α-Fe_2O_3/MWCNTs revealed high specific initial discharge capacity and preserved a stable discharge capacity with minimum capacity degradation [37]. The metal oxides are observed to have outstanding capacitance but low electrical conductivity and electrochemical stability that restrict their device applications [38]. The MWCNT-based $NiFe_2O_4$ nanohybrids were fabricated and high specific capacity, excellent rate capability, better cyclic performance by giving 97% columbic efficiency were found [39]. The tungsten (Ti)-decorated titania nanotubes, Au/TiO_2-WO_3 nanocomposites, Ti-based copper (Cu) nanotubes composites, and manganese- or cobalt-based TiO_2 nanocomposites were produced for the study of electrochemical properties [40, 41]. The $MnFe_2O_4$ nanoparticles showed remarkable specific capacitance at 5 mVs^{-1} and 25% retention was observed at 100 mVs^{-1} [42]. The $MnFe_2O_4$/graphene electrode materials showed sphere-like morphology and have notable electrochemical stability and better specific capacitance [43]. The $CuFe_2O_4$/rGO composites were synthesized using the thermo-chemical reaction method to examine the effects of rGOs on the structural, dielectric properties, and battery performance of $CuFe_2O_4$ nanoparticles. The $CuFe_2O_4$/rGO composites showed remarkably enhanced electrochemical properties with the addition of rGOs [44]. The $ZnFe_2O_4$ nanoparticles got higher theoretical capacity, but slow Li-ions diffusion and poor electrical conductivity restrict the rate capabilities for fast charge/discharge [45, 46]. The carbon was proved to be an inactive substance to alleviate the active constituent. The porous carbon, graphene ,and carbon nanotube-based composites with metal oxide nanoparticles dispersed in carbon matrix were investigated and it is an efficient approach to avoid aggregation of nanoparticles by chemical bonding [47–50]. In the present study, the $CrFe_2O_4$/$(MWCNTs)_x$; $x=0$, 5, 10, 15, and 20 wt% nanohybrids were synthesized by ultra-sonication-assisted route. The $CrFe_2O_4$ nanoparticles and MWCNTs were dispersed for the first time using toluene, a dispersive medium, for these nanohybrids. The electrochemical response of these nanohybrids was estimated by cyclic voltammetry and electrochemical impedance spectroscopy at room temperature.

2 Experimental

2.1 Material synthesis

The chemical co-precipitation route was adopted for the synthesis of $CrFe_2O_4$ nanoparticles. For this, 0.1 molarity solution of chromium nitrate {$\{Cr(NO_3)_2.9H_2O\}$} and 0.2 molarity solution of iron nitrate {$\{Fe(NO_3)_2.9H_2O\}$} were used and they were homogenously mixed by continuous stirring. The mixture was heated at 90 °C and a solution of 03 molarity sodium hydroxide (NaOH), which was previously heated to 80 °C, was added dropwise to the mixture and stirred for 50 min at 90 °C. The solution was then cooled to room temperature and washed several times with double-distilled water to achieve pH 7. The resultant solution was dried at 100 °C using microwave oven for 12 h followed by annealing at 500 °C for 4 h to get spinel phase $CrFe_2O_4$ nanoparticles. The product was ground in mortar and pestle to eliminate agglomeration. For the preparation of $CrFe_2O_4$/$(MWCNTs)_x$; $x=0$, 5, 10, 15, and 20 wt% nanohybrids, pre-acquired MWCNTs and $CrFe_2O_4$ nanoparticles were separately taken in 50 ml of toluene. For uniform dispersion, these were sonicated for 2 hrs at room temperature and then the $CrFe_2O_4$ nanoparticles were added into MWCNTs solutions. The mixture was again sonicated using ultra-bath sonicator for 6 hrs and, then, the solution was dried at 100 °C in a microwave oven. The dried product was annealed at 350 °C for 2 h and it was further homogenized using mechanical mixing to avoid any agglomeration to acquire $CrFe_2O_4$/$(MWCNTs)_x$; $x=0$, 5, 10, 15, and 20 wt% nanohybrids.

2.2 Characterization techniques

Powder X-rays Diffraction (XRD) with the use of CuKα (1.5405 Å) radiation was employed to investigate the phase formation and crystallinity of $CrFe_2O_4$ nanoparticles, MWCNTs, and $CrFe_2O_4$/$(MWCNTs)_x$ nanohybrids. Raman spectroscopy was monitored using Laser Confocal micro-Raman spectrometer with the aid of Renishaw Via-Reflex, equipped with 3 lasers having different wavelengths with resolution of 2 cm^{-1}. The morphology of $CrFe_2O_4$ nanoparticles, MWCNTs, and $CrFe_2O_4$/$(MWCNTs)_x$ nanohybrids was checked by SEM with the help of an JEOL-JSM 6390. An FTIR spectrometer Perkin Elmer was used to carry out FTIR spectroscopy of these nanohybrids in the range of 390–1800 cm^{-1} with the aid of KBr pellet technique.

2.3 Electrochemical measurements

The electrochemical measurements of $CrFe_2O_4$/$(MWCNTs)_x$; $x=0$, 5, 10, 15, and 20 wt% nanohybrids were carried out using coin-type cells with Li-foil as both the reference and counter electrode at room temperature. The working electrodes were prepared with the active material, conductive materials (acetylene black), and a polyvinylidene fluoride (PVDF) binder in weight ratio of 8:1:1. About 3 mg electrode materials were coated on a round copper with a diameter of 1 cm. The electrolyte was 1 M LiPF6 in a mixture of 50 vol% ethylene carbonate (EC) and 50 vol% dimethyl carbonate (DMC). A celgard 2325 microporous

membrane was used as a separator. The CR2025 coin-type cells were assembled in argon-filled glove box with the concentration of moisture and oxygen below 1.0 ppm. The cyclic voltammetry (CV) measurements of $CrFe_2O_4$/$(MWCNTs)_x$; $x = 0$, 5, 10, 15, and 20 wt% nanohybrids were performed on an electrochemical workstation (AMETEK, VMC-4) in the voltage range of 0–3.0 V and a scan rate of 0.1 mVs^{-1}. The electrochemical impedance spectroscopy (EIS) of $CrFe_2O_4$/$(MWCNTs)_x$ electrodes was tested in a frequency range from 0.01 Hz to 100 KHz.

3 Results and discussion

3.1 Structural investigations

XRD technique was used to explore phase formation and crystal structure of pristine MWCNTs and $CrFe_2O_4$/$(MWCNTs)_x$ nanohybrids. The XRD spectra of $CrFe_2O_4$/$(MWCNTs)_x$; $x = 0$, 5, 10, 15, and 20 wt% nanohybrids are shown in Fig. 1. The peaks at 30.2°, 35.6°, 37.5°, 43.6°, 53.7°, 57.2°, 62.6°, and 64.9° correspond to (220), (311), (222), (400), (422), (511), (440), and (433) planes established in the cubic FCC crystal structure for $CrFe_2O_4$ nanoparticles. The XRD pattern of pristine MWCNTs is given in the inset of Fig. 1, which shows two peaks at 25.2° and 42.4° corresponding to (002) and (100) planes, respectively. In Fig. 1, the characteristic peak for MWCNTs was obtained at 25.2° with (002) plane that corresponds to their graphitic reflection. The most intense peak at 35.6° attributed to the (311) plane of $CrFe_2O_4$ phase verifies the crystallinity of this component [51]. No additional peaks were observed in the samples and it confirms the absence of impurities in these nanohybrids. This described the entire attachment

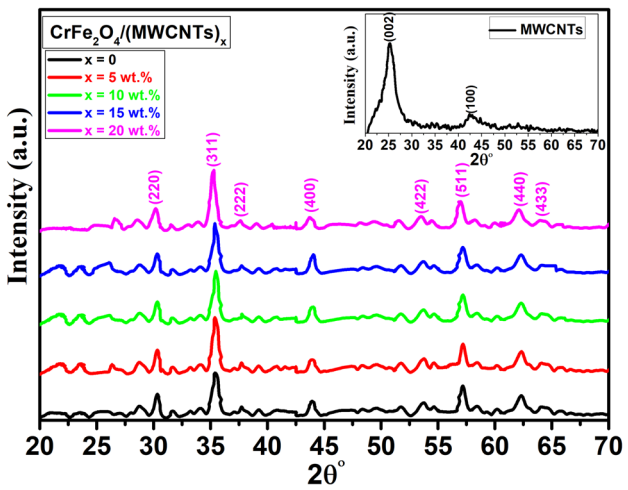

Fig. 1 XRD patterns of $CrFe_2O_4$/$(MWCNTs)_x$; $x = 0$, 5, 10, 15 & 20 wt% nanohybrids and in the set the XRD pattern of pristine MWCNT

of $CrFe_2O_4$ nanoparticles on MWCNTs, thus demonstrating uniform dispersion. The Debye-Scherrer formula was used to compute the crystallite size of $CrFe_2O_4$ nanoparticles using the intense peak of (311) plane and the value of 30 nm was found. The peak broadening with increasing the MWCNTs content indicates the adsorption of $CrFe_2O_4$ on MWCNTs and crystallite size decrease.

Raman spectroscopic investigations were carried out at room temperature to examine the disordered structures of the synthesized material. Raman spectra of $CrFe_2O_4$/MWCNTs nanohybrid is given in Fig. 2 a, which is further splitted into spectrum of $CrFe_2O_4$ nanoparticles (Fig. 2b) and MWCNTs (Fig. 2c). The Raman spectrum in Fig. 2a recognized three different spectral intervals below 700 cm^{-1}, which are owed to stretching vibrational modes of $CrFe_2O_4$ nanoparticles. The Raman intensity peaks around 473 and 685 cm^{-1} can be assigned to the characteristic peaks of the $CrFe_2O_4$ nanoparticles that are involved in symmetric stretching of oxygen atoms to metal ions in tetrahedral voids, frequently experienced in crystalline spinel nanostructures. The peak appeared at 336 cm^{-1} is assigned to E_g vibration mode and the peak appeared at 578 cm^{-1} is due to T_{2g} vibration mode. The Raman spectrum of $CrFe_2O_4$/MWCNTs nanohybrid shows prominent peaks in between 1200 and 1600 cm^{-1} range. The two peaks appeared at 1345 cm^{-1} and 1606 cm^{-1}, as shown in Fig. 2b, are basically assigned to the D and G bands that correspond to induced disorder of graphitic carbonaceous materials and the C-C stretching, respectively [31, 52]. Essentially, the intensity of bands indicates contribution of sp^2-hybridized carbon on nanoparticles' surface. It was reported in previous studies that carbon-coated $LiFePO_4$ gave very low D: G band intensity, which corresponded to enlarged electronic conductivity of the carbonaceous material owing to increased sp^2:sp^3 ratio in terms of carbon coordination, that results in enhanced electrochemical performance of composite electrodes [31, 53, 54]. Therefore, it is evident from Raman investigations of $CrFe_2O_4$ nanoparticles that the synthesized nanostructure is spinel as already established from the XRD analysis.

3.2 Scanning electron microscopy (SEM)

The SEM images of pristine MWCNTs and $CrFe_2O_4$/$(MWCNTs)_x$; $x = 0$, 10, and 20 wt% nanohybrids are given in Fig. 3a–d, respectively. The diameter of MWCNTs was estimated to be 30–35 nm, while $CrFe_2O_4$ nanoparticles were observed to be 32 nm in size, and that was further verified by using histogram and was found in good agreement with estimated crystallite size. Some agglomerations were also observed in SEM images that show nanoparticles coalescence due to diffusion of atoms. The SEM images of $CrFe_2O_4$/$(MWCNTs)_x$; $x = 10$ and 20 wt% nanohybrids showed that large number of nanoparticles is still embedded

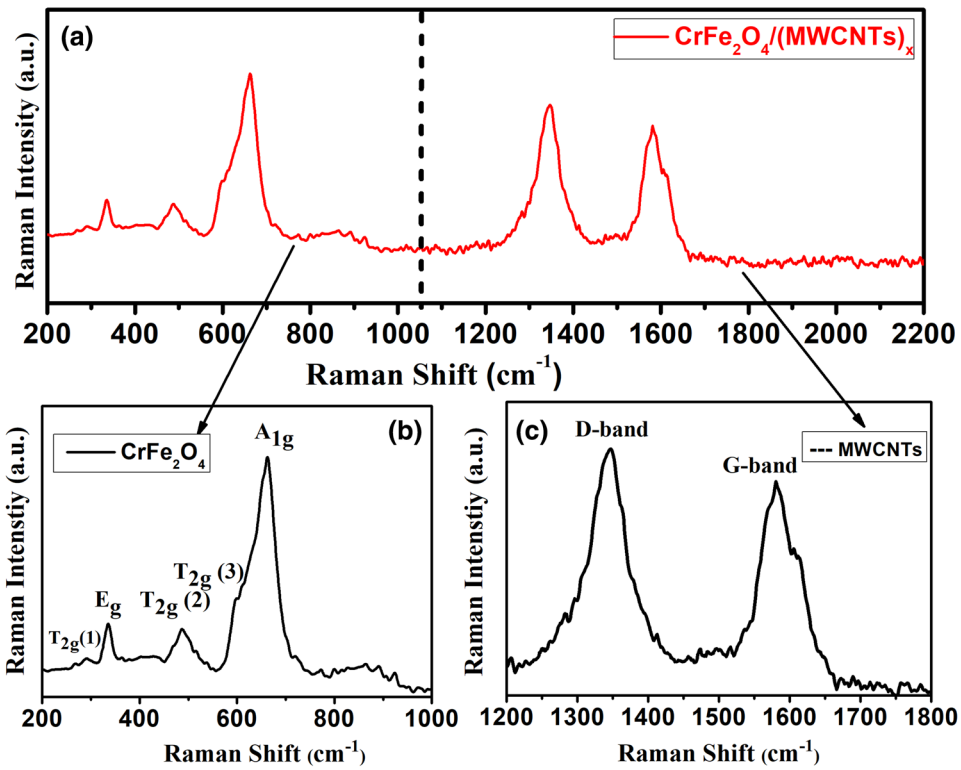

Fig. 2 Raman spectra of **a** $CrFe_2O_4/(MWCNTs)_x$ nanohybrids, **b** $CrFe_2O_4$ nanoparticles, and **c** MWCNTs, respectively

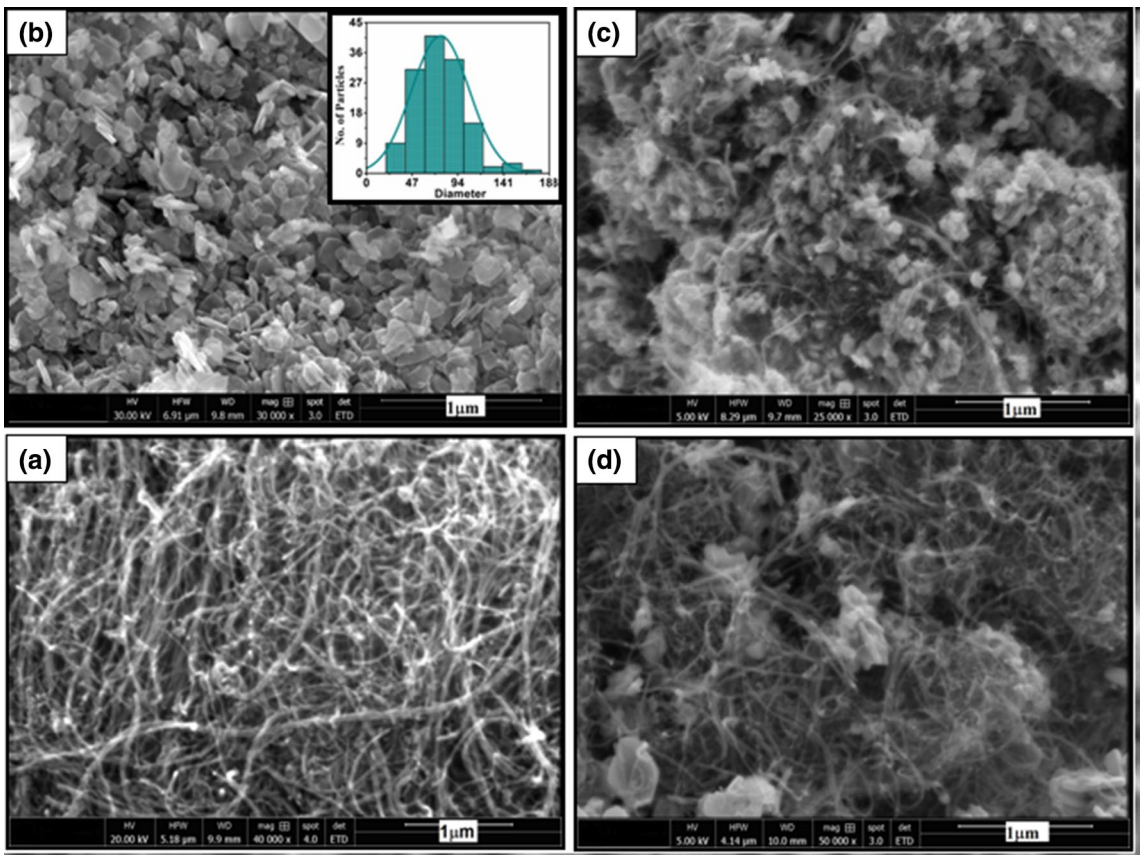

Fig. 3 **a** SEM image of pristine MWCNTs and **b**–**d** SEM images of $CrFe_2O_4/(MWCNTs)_x$ nanohybrids with $x = 0$, 10, and 20 wt%, respectively.

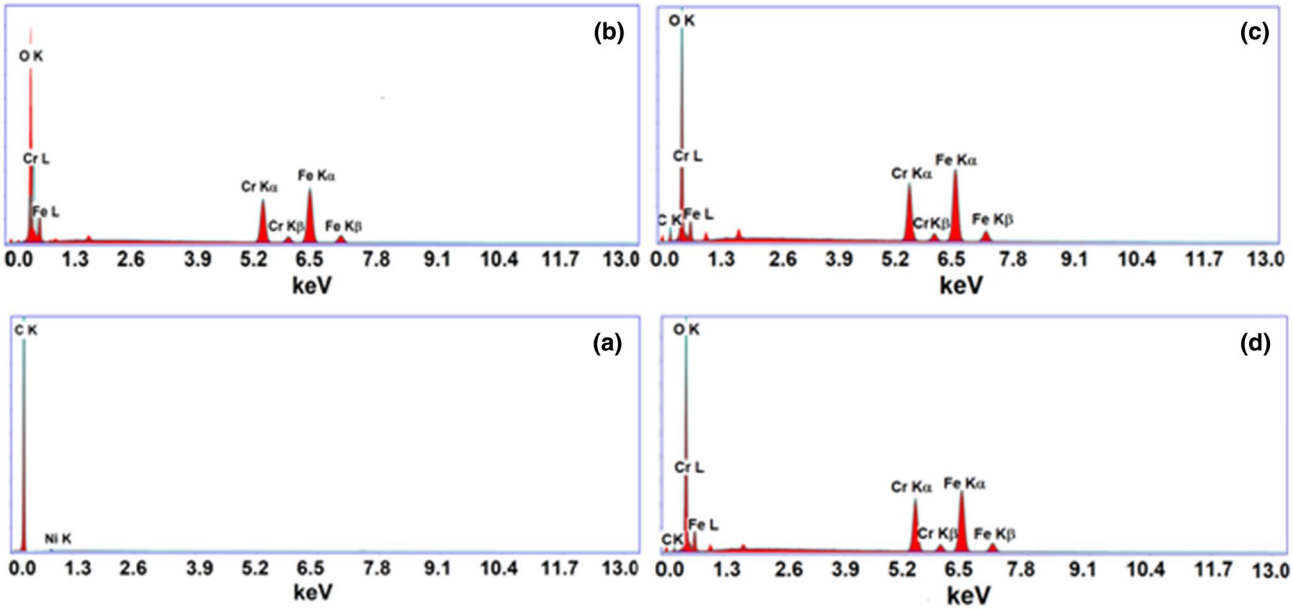

Fig. 4 **a** EDX spectrum of pristine MWCNTs and **b–d** EDX spectra of $CrFe_2O_4/(MWCNTs)_x$ nanohybrids with x = 0, 10, and 20 wt%, respectively

on MWCNTs owing to π–π interactions that signify the high efficiency of dispersion route.

3.3 Energy dispersive X-rays spectroscopy (EDX)

EDX is an analytical technique employed to study the elemental and chemical composition of a sample, which signifies that each element has distinct electronic structure leasing a unique set of peaks at its emission bands [55]. The EDX spectra of pristine MWCNTs and $CrFe_2O_4/(MWCNTs)_x$; x = 0, 10, and 20 wt% nanohybrids are shown in Fig. 4a–d. The element contents in these nanohybrids were experimentally estimated and they are listed in Table 1. It is evident from EDX spectra that there are no foreign elements observed, excepting the constituent components of Cr, Fe, O, and C in these nanohybrids.

3.4 Fourier transform infrared (FTIR) spectroscopy

The FTIR spectra of $CrFe_2O_4/(MWCNTs)_x$; x = 0, 5, 10, 15, and 20 wt% nanohybrids are shown in Fig. 5. The strong absorption modes at 398, 503, and 566 cm^{-1} of $CrFe_2O_4$ nanoparticles are basically representative for tetrahedral (A) and octahedral (B) sites. The metal-oxygen-elongated vibrational modes at A and B sites are basically attributed to these absorption modes. In FTIR spectra, the establishment of these two sublattices vibrational modes acknowledge single-phase spinal structure configuration [56–59]. A slight shift in vibrational modes was noticed with increasing contents of MWCNTs and it indicates the subsistence of

Table 1 Compositional analysis of pristine MWCNTs and $CrFe_2O_4/(MWCNTs)_x$; x = 0, 10, and 20 wt% nanohybrids.

$CrFe_2O_4/(MWCNTs)_x$ Nanohybrids	MWCNTs	0 wt%	10 wt%	20 wt%
Cr (wt%)	–	29.26	19.68	18.1
Fe (wt%)	–	50.02	43.48	43.2
O (wt%)	1.01	20.72	33.58	32.17
C (wt%)	98.99	–	3.26	6.53

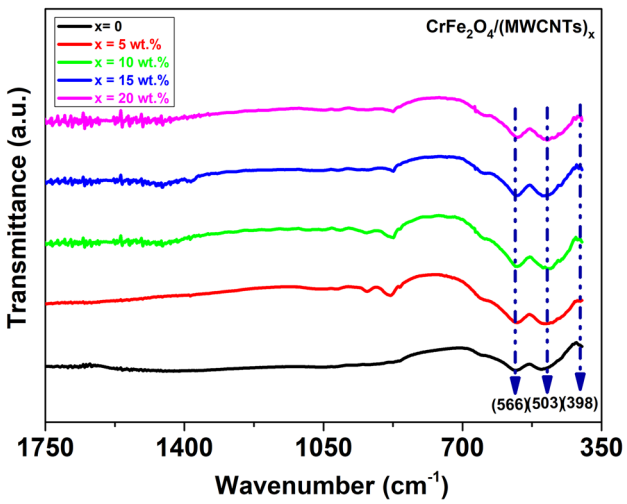

Fig. 5 FTIR spectra of $CrFe_2O_4/(MWCNTs)_x$; x = 0, 5, 10, 15, and 20 wt% nanohybrids

intermolecular forces between $CrFe_2O_4$ nanoparticles and MWCNTs.

3.5 Cyclic voltammetry (CV)

The electrochemical behavior of $CrFe_2O_4/(MWCNTs)_x$ nanohybrids was examined through recording cyclic voltammograms (CV) in voltage range of 0–3.0 V at 0.1 mVs^{-1} scan rate. The CV curves of $CrFe_2O_4/(MWCNTs)_x$; $x = 0$, 5, 10, 15, and 20 wt% nanohybrids obtained for 5 cycles are given in Fig. 6a–e. In CV curves, the peak that appears in the negative current regime is called cathodic (reduction) peak, while the peak that emerges in the positive current region is termed as an anodic (oxidation) peak. It is evident from the CV curves of $CrFe_2O_4/(MWCNTs)_x$; $x = 0$, 5, 10, 15, and 20 wt% electrodes that a small peak appeared at 2.3 V in anodic scan ascribed the existence of side reactions on electrode surfaces. Furthermore, the irreversible decomposition of electrolyte at interfaces caused the formation of a solid electrolyte interphase (SEI). The reduction peak at 0.4 V is attributed to the reduction of $CrFe_2O_4$ nanoparticles to Cr, Fe, and establishment of Li_2O. In subsequent cycles, the cathodic peak shifts towards low potential, whereas the anodic peak shifted towards higher potential, which suggests the structural and lithium-driven alterations during cathodic and anodic processes [60]. The peak current and area under CV curves did not show any significant diminishing behavior with the increased number of cycles that shows good capacitive conduction and charge storage ability of the working electrodes. The reversible peaks experienced beneath 0.4 V correspond to Li-ion intercalation or de-intercalation processes [45, 61–64]. In the CV curves of $CrFe_2O_4/(MWCNTs)_x$ electrodes, the existence of redox peaks

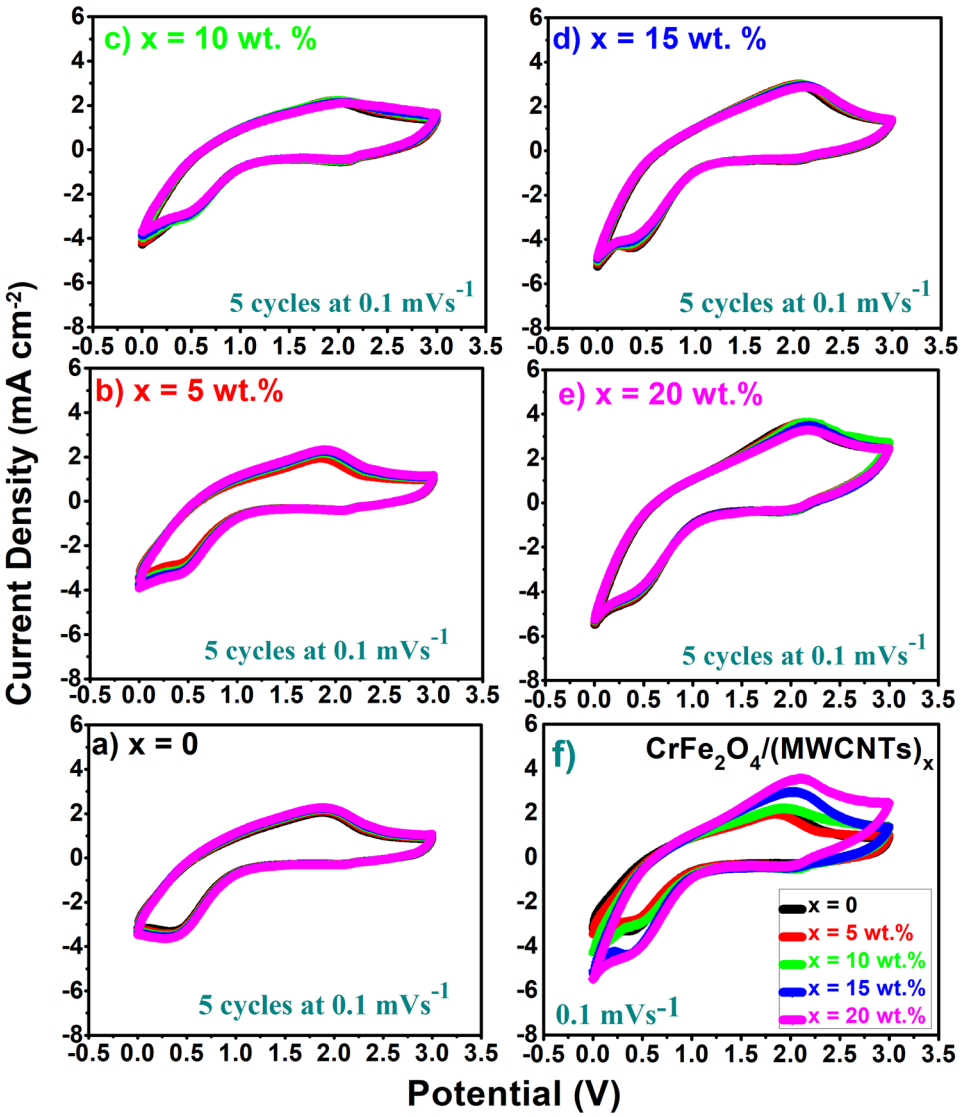

Fig. 6 The 5 cycles of CV for $CrFe_2O_4/(MWCNTs)x$ nanohybrids with **a** $x = 0$, **b** $x = 5$, **c** $x = 10$, **d** $x = 15$, and **e** $x = 20$ wt%, respectively, and **f** One cycle of CV for $CrFe_2O_4/(MWCNTs)_x$; $x = 0$, 5, 10, 15, and 20 wt% nanohybrids.

revealed the pseudo-capacitive conduction of $CrFe_2O_4$, which is considerable in entire specific capacitance (C_s) of the electrodes. The redox reactions of $CrFe_2O_4$ nanoparticles are illustrated below:

$$CrFe_2O_4 + 8Li^+ + 8e^- \leftrightarrow Cr + Fe + 4Li_2O$$

$$Cr + Li^+ + e^- \leftrightarrow LiZn$$

$$Fe_2O_3 + 6Li^+ + 6e^- \leftrightarrow Fe + 3Li_2O$$

For the $CrFe_2O_4/(MWCNTs)_x$; $x = 0$, 5, 10, 15, and 20 wt% electrodes, both the oxidation and reduction peaks are positively shifted with increased loadings of MWCNTs as shown in Fig. 6f, that is caused by structural rearrangement of the electrode materials and increased polarization [65]. It is clear from Fig. 6f that the curves show almost similar shaped peaks. However, the integrated peak area and peak currents of $CrFe_2O_4/(MWCNTs)_x$; $x = 5$, 10, 15, and 20 wt% electrodes are much higher, as compared to those of bare $CrFe_2O_4$, which indicates that the bare electrode has high reactivity and capacity. Moreover, the reduction peak of bare $CrFe_2O_4$ was found at about 0.40 V, whereas the reduction peaks of $CrFe_2O_4/(MWCNTs)_x$ nanohybrids were recorded at a lower potential (i.e.; ~ 0.36 V), which implies that nanohybrids have large irreversible capacity. It was observed that the values of peak-to-peak potential (E_{pp}) increase with increasing contents of MWCNTs in $CrFe_2O_4/(MWCNTs)_x$ electrodes, as shown in Fig. 7. The area under the CV curves increases linearly with increasing content of MWCNTs, which indicates that maximum electrode active surfaces are accessible with excellent electrical conductivity. The specific capacitance 'C_s' (F/g) of working electrode was estimated by the following relation [66]:

$$C_s = \frac{\Delta I}{m \times s}$$

where ΔI (A) is the difference of oxidation and reduction peak currents in amperes, m (g) is the loading mass, and s (mVs^{-1}) is the scan rate. The variation in C_s with number of cycles for working electrode of $CrFe_2O_4/(MWCNTs)_x$ nanohybrids is shown in Fig. 8. It is obvious that C_s decreases with increasing number of cycles, while it is increased with increasing contents of MWCNTs. This may be due to the passage of maximum number of ions through the electrode, while the interaction between electro-active materials and ions became frail that leads C_s to lower values. It is also evident from Fig. 8 that the values of C_s for synthesized $CrFe_2O_4/(MWCNTs)_x$ nanohybrids are found to be greater with increased loadings of MWCNTs as compared to bare $CrFe_2O_4$ nanoparticles. Thus, this study can be helpful to estimate the capacitance retention in a material subsequent to certain number of cycles.

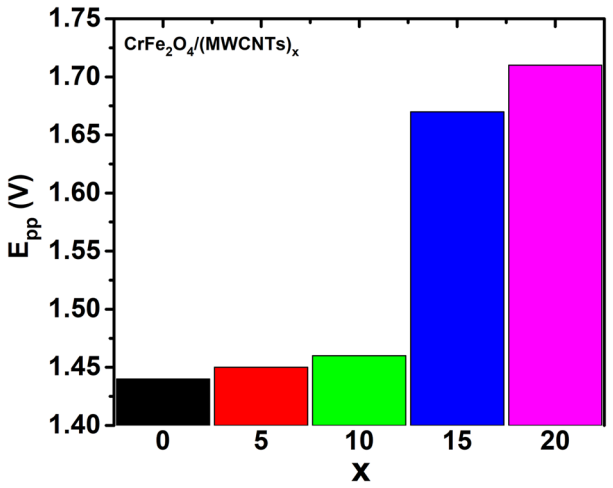

Fig. 7 Variation of Epp versus MWCNTs contents (x) in $CrFe_2O_4/(MWCNTs)_x$; $x = 0$, 5, 10, 15, and 20 wt% nanohybrids.

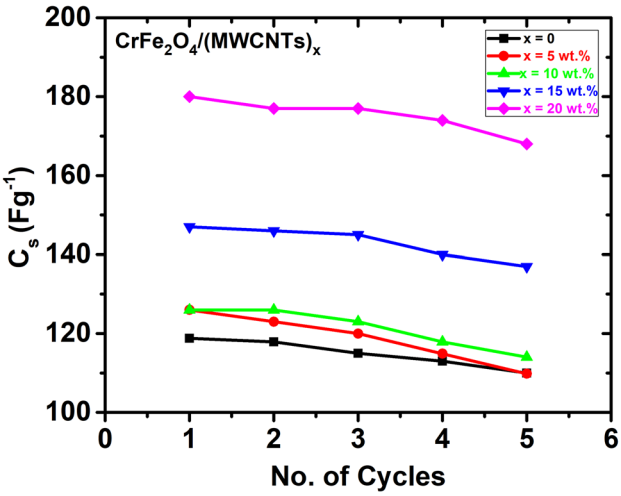

Fig. 8 Variation of Cs versus No. of cycles of $CrFe_2O_4/(MWCNTs)_x$; $x = 0$, 5, 10, 15, and 20 wt% nanohybrids

3.6 Electrochemical impedance spectroscopy (EIS)

The electrochemical impedance spectroscopy (EIS) of these synthesized electrodes was conducted to estimate the charge transfer resistance with the aid of Nyquist plots. Generally, in Nyquist plots, the semicircle at high frequency gives charge transfer resistance, while, at low frequency, a straight line appeared that is associated with diverse diffusion-controlled processes that happened a electrode interfaces [67]. Usually, it was noticed that the diameter of semicircle in the Nyquist plots is assigned to the charge transfer resistance (R_{ct}) and it will be higher when the diameter of semicircle is greater. The Nyquist plots of $CrFe_2O_4/(MWCNTs)_x$; $x = 0$, 5, 10, 15, and 20 wt% electrodes are shown in Fig. 9.

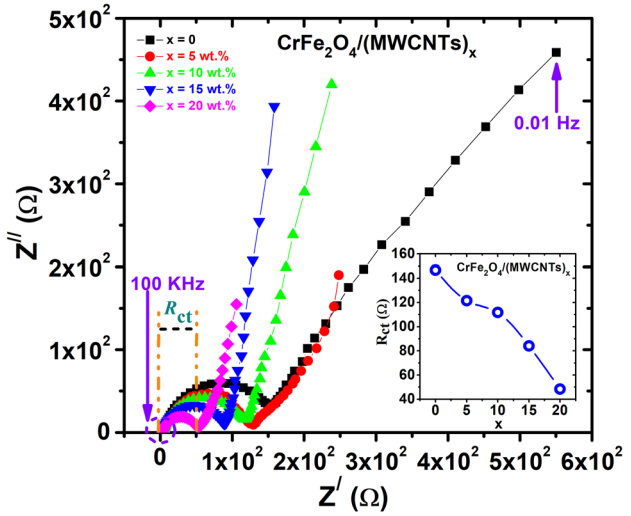

Fig. 9 Nyquist plots of $CrFe_2O_4/(MWCNTs)_x$; x = 0, 5, 10, 15, and 20 wt% nanohybrids in a frequency range from 0.01 Hz to 100 KHz.

The decrease in semicircle diameter of these electrodes was observed with increased loadings of MWCNTs, and that showed the enhanced electrochemical behavior. The inset of Fig. 9 showed that R_{ct} got high value for bare $CrFe_2O_4$ electrode that was deceased with increasing contents of MWCNTs. This may be due to good inter-particle electrical contact between nanoparticles and MWCNTs, and thus, the decreased electrical resistivity can be reached. It may also indicate that MWCNTs blocks easy incursion of lithium ions into nanoparticles. Hence, the outcomes exhibit that $CrFe_2O_4/(MWCNTs)_x$; x=0, 5, 10, 15, and 20 wt% nanohybrids are useful composites to improve the electrochemical performance of Li-ion batteries.

4 Conclusions

The $CrFe_2O_4/(MWCNTs)_x$ nanohybrids were successfully synthesized by novel two-step route. First, the bare $CrFe_2O_4$ nanoparticles were produced by chemical co-precipitation route that were later embedded on the surface of MWCNTs by ultra-sonication-assisted route. The toluene was used as dispersive medium for the first time during synthesis of these nanohybrids. The capacitive performance of these nanohybrids was studied by performing CV experiments and EIS measurements. The CV curves showed that $CrFe_2O_4/(MWCNTs)_x$ nanohybrids got higher C_s as compared to bare $CrFe_2O_4$ electrode. Moreover, C_s of $CrFe_2O_4/(MWCNTs)_x$ nanohybrids was found decreasing with increasing number of cycles that maybe due to the passage of maximum number of ions through the electrode, while the interaction became frail between electro-active material and the ions. The Nyquist plot of $CrFe_2O_4$ showed greater value of R_{ct} as compared to that of MWCNT-based nanohybrids, which indicated the enhanced electrochemical behavior. It was also observed that bare $CrFe_2O_4$ electrode exhibited higher value of R_{ct}, which was deceased with increasing contents of MWCNTs due to good inter-particle electrical contact between nanoparticles and MWCNTs. These results indicate that $CrFe_2O_4/(MWCNTs)_x$ nanohybrids are the potential candidates for the high-performance energy storage devices especially for Li-ion batteries.

References

1. T. Kozawa, T. Murakami, M. Naito, Insertion of lattice strains into ordered $LiNi_{0.5}Mn_{1.5}O_4$ spinel by mechanical stress: a comparison of perfect versus imperfect structures as a cathode for Li-ion batteries. J. Power Sources **320**, 120–126 (2016)
2. F. Tao, Y.Q. Zhao, G.Q. Zhang, H.L. Li, Electrochemical characterization on cobalt sulfide for electrochemical supercapacitors. Electrochem. Commun. **9**, 1282–1287 (2007)
3. Y. Qi, Y. Huang, D. Jia, S.J. Bao, Z.P. Guo, Preparation and characterization of novel spinel $Li_4Ti_5O_{12-x}Br_x$ anode material. Electrochim. Acta **54**, 4772–4776 (2009)
4. B. Bhujun, M.T. Tan, A.S. Shanmugam, Study of mixed ternary transition metal ferrites as potential electrodes for supercapacitor applications. Results Phys. **7**, 345–353 (2017)
5. J.B. Goodenough, Y. Kim, Challenges for rechargeable Li batteries. Chem. Mater. **22**, 587–603 (2010)
6. J.M. Tarascon, M. Armand, Issues and challenges facing rechargeable lithium batteries. Nature **414**, 359–367 (2001)
7. B. Dunn, H. Kamath, J.M. Tarascon, Electrical energy storage for the grid: a battery of choices. Science **334**, 928–935 (2011)
8. H. Su, H. Zhang, F. Liu, F. Chun, B. Zhang, X. Chu, H. Huang, W. Deng, B. Gu, H. Zhang, X. Zheng, M. Zhu, W. Yang, High power supercapacitors based on hierarchically porous sheet-like nanocarbons with ionic liquid electrolytes. Chem. Eng. J. **322**, 73–81 (2017)
9. L.C. Yang, Q.S. Gao, Y.H. Zhang, Y. Tang, Y.P. Wu, Tremella-like molybdenum dioxide consisting of nanosheets as an anode material for lithium ion battery. Electrochem. Commun. **10**, 118–122 (2008)
10. H.B. Wu, J.S. Chen, H.H. Hng, X.W. Lou, Nanostructured metal oxide based materials as advanced anodes for lithium-ion batteries. Nanoscale **4**, 2526–2542 (2012)
11. G. Li, R. Li, W. Zhou, A wire-shaped supercapacitor in micrometer size based on Fe_3O_4 nanosheet arrays on Fe wire. Nano Micro Lett. **9**, 46 (2017)
12. T.V. Solís, P.V. Vigón, S. Álvarez, G. Marbán, A.B. Fuertes, Manganese ferrite nanoparticles synthesized through a nanocasting route as a highly active fenton catalyst. Catal. Commun. **8**, 2037–2042 (2007)
13. D. Ling, N. Lee, T. Hyeon, Chemical synthesis and assembly of uniformly sized iron oxide nanoparticles for medical applications. Acc. Chem. Res. **48**, 1276–1285 (2015)
14. T. Namsaraeva, B. Bazarov, D. Mikhailova, N. Kuratieva, A. Sarapulova, A. Senyshyn, H. Ehrenberg, Orthomolybdates in the Cs–FeII, III–Mo–O System: Cs4Fe(MoO4)3, Cs2Fe2(MoO4)3 and CsFe5(MoO4)7. Eur. J. Inorg. Chem. **2011**, 2832–2841 (2011)
15. V.V. Atuchin, D.A. Vinnik, T.A. Gavrilova, S.A. Gudkova, L.I. Isaenko, X. Jiang, L.D. Pokrovsky, I.P. Prosvirin, L.S. Mashkovtseva, Z. Lin, Flux crystal growth and the electronic structure of $BaFe_{12}O_{19}$ hexaferrite. J. Phys. Chem. C **120**, 5114–5123 (2016)

16. M.N. Timofeeva, V.N. Panchenko, N.A. Khan, Z. Hasan, I.P. Prosvirin, S.V. Tsybulya, S.H. Jhung, Isostructural metal-carboxylates MIL-100(M) and MIL-53(M) (M: V, Al, Fe and Cr) as catalysts for condensation of glycerol with acetone. Appl. Catal. A General **529**, 167–174 (2017)
17. D.A. Vinnik, D.S. Klygach, V.E. Zhivulin, A.I. Malkin, M.G. Vakhitov, S.A. Gudkova, D.M. Galimov, D.A. Zherebtsov, E.A. Trofimov, N.S. Knyazev, V.V. Atuchin, S.V. Trukhanov, A.V. Trukhanov, Electromagnetic properties of $BaFe_{12}O_{19}$:Ti at centimeter wavelengths. J. Alloy Compd. **755**, 177–183 (2018)
18. Z. Zhang, Y. Wang, Q. Tan, Z. Zhong, F. Su, Facile solvothermal synthesis of mesoporous manganese ferrite ($MnFe_2O_4$) microspheres as anode materials for lithium-ion batteries. J. Colloid Interface Sci. **398**, 185–192 (2013)
19. X. Hou, J. Feng, Y. Ren, Z. Fan, M. Zhang, Synthesis and adsorption properties of sponge like porous $MnFe_2O_4$. Colloids Surf. A **363**, 1–7 (2010)
20. R. Wang, Q. Li, L. Cheng, H. Li, B. Wang, X.S. Zhao, P. Guo, Electrochemical properties of manganese ferrite based supercapacitors in aqueous electrolyte: the effect of ionic radius. Colloids Surf. A **457**, 94–99 (2014)
21. J. Azadmanjiri, Preparation of Mn-Zn ferrite nanoparticles from chemical sol-gel combustion method and the magnetic properties after sintering. J. Non-Cryst. Solids **353**, 4170–4173 (2007)
22. T.H. Ko, D. Lei, S. Balasubramaniam, M.K. Seo, Y.S. Chung, H.Y. Kim, B.S. Kim, Polypyrrole decorated hierarchical $NiCo_2O_4$ nanoneedles/carbon fiber papers for flexible high performance supercapacitor applications. Electrochim. Acta **247**, 524–534 (2017)
23. G. Cai, P. Darmawan, M. Cui, J. Wang, J. Chen, S. Magdassi, P.S. Lee, Highly stable transparent conductive silver grid/PEDOT:PSS electrodes for integrated bifunctional flexible electrochromic supercapacitors. Adv. Energy Mater. **6**, 1–8 (2016)
24. A. Eftekhari, L. Li, Y. Yang, Polyaniline supercapacitors. J. Power Sources **347**, 86–107 (2017)
25. F. Liu, H. Su, L. Jin, H. Zhang, X. Chu, W. Yang, Facile synthesis of ultrafine cobalt oxide nanoparticles for high performance supercapacitors. J. Colloid Interface Sci. **505**, 796–804 (2017)
26. Y. Yang, J. Li, D. Chen, J. Zhao, A facile electrophoretic deposition route to the Fe_3O_4/CNTs/rGO composite electrode as a binder free anode for lithium ion battery. ACS Appl. Mater. Interfaces **8**, 26730–26739 (2016)
27. N. Pramanik, J. De, R.K. Basu, T. Rath, P.P. Kundu, Fabrication of magnetite nanoparticle doped reduced graphene oxide grafted polyhydroxyalkanoate nanocomposites for tissue engineering application. RSC Adv. **6**, 46116–46133 (2016)
28. P. Bhattacharya, S. Dhibar, G. Hatui, A. Mandal, T. Das, C.K. Das, Graphene decorated with hexagonal shaped M-type ferrite and polyaniline wrapper: a potential candidate for electromagnetic wave absorbing and energy storage device applications. RSC Adv. **4**, 17039–17053 (2014)
29. W. Zhang, B. Quan, C. Lee, S.K. Park, X. Li, E. Choi, G. Diao, Y. Piao, One step facile solvothermal synthesis of copper ferrite-graphene composite as a high performance supercapacitor material. ACS Appl. Mater. Interfaces **7**, 2404–2414 (2015)
30. L. Wang, L. Zhuo, H. Cheng, C. Zhang, F. Zhao, Porous carbon nanotubes decorated with nanosized cobalt ferrite as anode materials for high-performance lithium ion batteries. J. Power Sources **283**, 289–299 (2015)
31. M.W. Khan, X. Zuo, Q. Yang, H. Tang, K.M. Rehman, M. Wu, G. Li, Functionalized multi-walled carbon nanotubes embedded with nanoflakes boost the short-circuit current of Ru (II) based dye-sensitized solar cells. Dyes Pigments **181**, 108573 (2020)
32. J. Cai, H. Niu, H. Wang, H. Shao, J. Fang, J. He, H. Xiong, C. Ma, T. Lin, High performance supercapacitor electrode from cellulose derived, inter-bonded carbon nanofibers. J. Power Sources **324**, 302–308 (2016)
33. K.V. Dorozhkin, G.E. Dunaevsky, SYu. Sarkisov, V.I. Suslyaev, O.P. Tolbanov, V.A. Zhuravlev, Yu.S. Sarkisov, V.L. Kuznetsov, S.I. Moseenkov, N.V. Semikolenova, V.A. Zakharov, V.V. Atuchin, Terahertz dielectric properties of multiwalled carbon nanotube/polyethylene composites. Mater. Res. Express **4**, 106201 (2017)
34. M. Raghasudha, D. Ravinder, P. Veerasomaiah, FTIR studies and dielectric properties of Cr substituted cobalt nano ferrites synthesized by citrate-gel method. Nanosci. Nanotechnol. **3**, 105–114 (2013)
35. M.M. Abdullah, F.M. Rajab, S.M. Abbas, Structurally and optical characterization of Cr_2O_3 nanostructures: evaluation of its dielectric properties. AIP Adv. **4**, 027121–027111 (2014)
36. R.K. Sharma, O. Suwalka, N. Lakshmi, K. Venugopalan, A. Banerjee, P.A. Joy, Synthesis of chromium substituted nano particles of cobalt zinc ferrites by coprecipitation. Mater. Lett. **59**, 3402–3405 (2005)
37. Y. Huang, Z. Dong, D. Jia, Z. Guo, W.I. Cho, Electrochemical properties of α-Fe_2O_3/MWCNTs as anode materials for lithium-ion batteries. Solid State Ion. **201**, 54–59 (2011)
38. S. Chu, A. Majumdar, Opportunities and challenges for a sustainable energy future. Nature **488**, 294–303 (2012)
39. M. Mujahid, R.U. Khan, M. Mumtaz, S.A. Mubasher, Soomro, S. Ullah, $NiFe_2O_4$ nanoparticles/MWCNTs nanohybrid as anode material for lithium-ion battery. Ceram. Int. **45**, 8486–8493 (2019)
40. M.M. Momeni, Y. Ghayeb, Fabrication, characterization and photocatalytic properties of Au/TiO_2-WO_3 nanotubular composite synthesized by photo assisted deposition and electrochemical anodizing methods. J. Mol. Catal. A Chem. **417**, 107–115 (2016)
41. M.M. Momeni, Z. Nazari, A. Kazempour, M. Hakimiyan, S.M. Mirhoseini, Preparation of CuO nanostructures coating on copper as supercapacitor materials. Surf. Eng. **30**, 775–778 (2014)
42. B. Bashir, W. Shaheen, M. Asghar, M.F. Warsi, M.A. Khan, S. Haider, I. Shakir, M. Shahid, Copper doped manganese ferrites nanoparticles anchored on graphene nanosheets for high performance energy storage applications. J. Alloy Compd. **695**, 881–887 (2017)
43. W. Cai, T. Lai, W. Dai, J. Ye, A facile approach to fabricate flexible all solid state supercapacitors based on $MnFe_2O_4$/graphene hybrids. J. Power Sources **255**, 170–178 (2014)
44. S.A. Soomro, I.H. Gul, H. Naseer, S.U. Marwat, M. Mujahid, Improved performance of CuFe24. Curr. Nanosci. **15**, 420–429 (2019)
45. D. Bresser, E. Paillard, R. Kloepsch, S. Krueger, M. Fiedler, R. Schmitz, D. Baither, M. Winter, S. Passerini, Carbon coated ZnFe24. Adv. Energy Mater. **3**, 513–523 (2013)
46. Y. Deng, Q. Zhang, S. Tang, L. Zhang, S. Deng, Z. Shi, G. Chen, One pot synthesis of ZnFe24. Chem. Commun. **47**, 6828–6830 (2011)
47. C. Casas, W. Li, A review of application of carbon nanotubes for lithium ion battery anode material. J. Power Sources **208**, 74–85 (2012)
48. W. Sun, Y. Wang, Graphene based nanocomposite anodes for lithium ion batteries. Nanoscale **6**, 11528–11552 (2014)
49. B. Jang, B.O. Chae, S. Park, J. Ha, S.M. Oh, H.B. Na, Y. Piao, Solventless synthesis of an iron-oxide/graphene nanocomposite and its application as an anode in high rate Li-ion batteries. J. Mater. Chem. A **1**, 15442–15446 (2013)
50. Y. Li, Q. Zhang, J. Zhu, X. Wei, P. Shen, An extremely stable MnO2. J. Mater. Chem. A **2**, 3163–3168 (2014)
51. Mubasher, M. Mumtaz, L. Hassan, Z. Ali, M.A. Ahmad, M.F. Imtiaz, A. Aamir, Rehman, K. Nadeem, Comparative study of frequency–dependent dielectric properties of ferrites MFe_2O_4 (M

= Co, Mg, Cr and Mn) nanoparticles. Appl. Phys. A **126**, 334 (2020)
52. R.B. Hadjean, J.P. Ramos, Raman microspectrometry applied to the study of electrode materials for lithium batteries. Chem. Rev. **110**, 1278–1319 (2010)
53. M.M. Doeff, Y. Hu, F. McLarnon, R. Kostecki, Effect of surface carbon structure on the electrochemical performance of LiFePO4. Electrochem. Solid State Lett. **6**, 207–209 (2003)
54. J.D. Wilcox, M.M. Doeff, M. Marcinek, R. Kostecki, Factors influencing the quality of carbon coatings on LiFePO4. J. Electrochem. Soc. **154**, 389–395 (2007)
55. R. Saravanan, *Ferrite Materials for Memory Applications*, 18th edn. (Materials Research Forum, Millersville, 2017)
56. S.A. Soomro, I.H. Gul, M.Z. Khan, H. Naseer, A.N. Khan, Dielectric properties evaluation of NiFe24. Ceram. Int. **43**, 4090–4095 (2017)
57. D.Q. Yang, B. Hennequin, E. Sacher, XPS demonstration of π-π interaction between benzyl mercaptan and multiwalled carbon nanotubes and their use in the adhesion of Pt nanoparticles. Chem. Mater. **18**, 5033–5038 (2006)
58. B.P. Singh, V. Choudhary, S. Teotia, T.K. Gupta, V. Nand, S.R.D. Singh, R.B. Mathur, Solvent free, efficient, industrially viable, fast dispersion process based amine modified MWCNT reinforced epoxy composites of superior mechanical properties. Adv. Mater. Lett. **6**, 104–113 (2015)
59. Q. Guan, Y. Li, Y. Chen, Y. Shi, J. Gu, B. Li, R. Miao, Q. Chen, P. Ning, Sulfonated multi-walled carbon nanotubes for biodiesel production through triglycerides transesterification. RSC Adv. **7**, 7250–7258 (2017)
60. Y.N. Li, R. Zeng, P. Zhang, Z.P. Guo, H. Liu, Controlled synthesis of α-Fe_2O_3 nanostructures and their size-dependent electrochemical properties for lithium-ion batteries. J. Power Sources **184**, 456–461 (2008)
61. J. Sui, C. Zhang, D. Hong, J. Li, Q. Cheng, Z. Li, W. Cai, Facile synthesis of MWCNT-ZnFe24. J. Mater. Chem. **22**, 13674–13681 (2012)
62. X. Yao, C. Zhao, J. Kong, H. Wu, D. Zhou, X. Lu, Dopamine assisted one pot synthesis of zinc ferrite embedded porous carbon nanospheres for ultrafast and stable lithium ion batteries. Chem. Commun. **50**, 14597–14600 (2014)
63. L. Lin, Q. Pan, ZnFe24. J. Mater. Chem. A **3**, 1724–1729 (2015)
64. J. Cai, C. Wu, Y. Zhu, P.K. Shen, K. Zhang, Hierarchical porous acetylene black/ZnFe24. Electrochim. Acta **187**, 584–592 (2015)
65. L. Ji, Z. Tan, T.R. Kuykendall, S. Aloni, S. Xun, E. Lin, V. Battaglia, Y. Zhang, Fe34. Phys. Chem. Chem. Phys. **13**, 7170–7177 (2011)
66. M.L. Aparna, A.N. Grace, P. Sathyanarayanan, N.K. Sahu, A comparative study on the supercapacitive behaviour of solvothermally prepared metal ferrite (MFe_2O_4, M = Fe, Co, Ni, Mn, Cu, Zn) nanoassemblies. J. Alloy Compd. **745**, 385–395 (2018)
67. A.K. Das, S.K. Karan, B.B. Khatua, High energy density ternary composite electrode material based on polyaniline (PANI), molybdenum trioxide (MoO3. Electrochim. Acta **180**, 1–15 (2015)